

Accepted Manuscript

Constitutive modelling of plasticity of fcc metals under extremely high strain rates

C.Y. Gao, L.C. Zhang

PII: S0749-6419(11)00191-4
DOI: [10.1016/j.ijplas.2011.12.001](https://doi.org/10.1016/j.ijplas.2011.12.001)
Reference: INTPLA 1475

To appear in: *International Journal of Plasticity*

Received Date: 10 August 2011
Revised Date: 30 November 2011

Please cite this article as: Gao, C.Y., Zhang, L.C., Constitutive modelling of plasticity of fcc metals under extremely high strain rates, *International Journal of Plasticity* (2011), doi: [10.1016/j.ijplas.2011.12.001](https://doi.org/10.1016/j.ijplas.2011.12.001)

This is a PDF file of an unedited manuscript that has been accepted for publication. As a service to our customers we are providing this early version of the manuscript. The manuscript will undergo copyediting, typesetting, and review of the resulting proof before it is published in its final form. Please note that during the production process errors may be discovered which could affect the content, and all legal disclaimers that apply to the journal pertain.



Constitutive modelling of plasticity of fcc metals under extremely high strain rates

C.Y. Gao[†], L.C. Zhang^{*}

School of Mechanical and Manufacturing Engineering, The University of New South Wales, NSW 2052, Australia

ABSTRACT

A reliable and accurate description of the constitutive behavior of metals under the coupled effect of extremely high strain rate has become more and more important. The conventional constitutive models available, however, do not apply when the strain rate is beyond $10^4 s^{-1}$. This paper establishes a new constitutive model to describe the fcc crystalline plasticity at the extreme strain rate beyond which the material sensitivity to strain rate increases dramatically. The new model distinguishes the mobile dislocations from the total dislocations and incorporates the change of mobile dislocation density to count for the microstructural evolution of the material. A unified constitutive model is then proposed. An optimization method was used to obtain globally optimal parameters in the model. The flow stress predictions by the unified model show a very good agreement with experiments within the whole strain rate range from $1 \times 10^{-4} s^{-1}$ to $6.4 \times 10^5 s^{-1}$. The flow stress upturn phenomenon in OFHC copper was satisfactorily described.

Keywords: constitutive modelling; fcc crystal plasticity; microstructural evolution; mobile dislocation density; extremely high strain rate

[†] On leave from the Department of Mechanics, Zhejiang University, Hangzhou, 310027, China

^{*} Corresponding author: Phone: + 61 2 9385 6078; Fax: + 61 2 9385 7316.

E-mail address: Liangchi.Zhang@unsw.edu.au

1. Introduction

The dynamic yield stress of a metal can be generally described by a function of plastic strain, strain rate, temperature, and internal state variables related to the structural evolution of the material. Various empirical constitutive models for dynamic plasticity have been proposed in past decades. There are two types of constitutive models: one is the high-pressure type which considers the pressure effect of strong shock and is established on the one-dimensional-strain experiments like pressure-shear plate impact test. The other is the regular-pressure type which does not need to include the pressure state variable and is established on the one-dimensional-stress experiments like Split Hopkinson Pressure Bar (SHPB) test. The distinct states of stress and strain in the two types of experiments may result in different plastic deformation mechanism since the deviatoric stress and pressure induce different microstructural responses in materials (Meyers, 1994). The high-pressure models, as reviewed by Remington et al. (2006), include the Steinberg-Guinan (SG) model (1980), the Steinberg-Lund (SL) model (1989) and the Preston-Tonks-Wallace (PTW) model (2003). The regular-pressure models, as reviewed by Chaboche (2008) and Lin and Chen (2011), include the widely used Johnson-Cook (JC) model (1985), the Khan-Huang-Liang (KHL) model (Khan and Huang, 1992; Khan and Liang, 1999; Khan et al., 2004) and the Hollomon/Voce (H/V) model (Sung et al., 2010). This paper will focus on the regular-pressure models. It was found that these empirical models cannot properly describe some experimental observations, particularly when a metal deforms under a very high strain rate, such as $10^4 - 10^6 s^{-1}$ in the case of high speed machining (Arsecularatne and Zhang, 2004). This is because the dynamic behavior of a metal at high strain rates is closely related

1 to its microstructural evolution during deformation, which is not considered in a conventional
2
3 phenomenological theory. Physically based constitutive models have therefore been
4
5 developed to fill the gap.
6
7

8
9 Zerilli and Armstrong (1987) proposed a constitutive relation using the thermal activation
10 analysis of dislocation motion. They found that the dislocation mechanisms in metals of
11 different crystalline structures were different. For face-centered cubic (fcc) metals,
12 dislocations must traverse the barriers of forest dislocations, and the thermal activation area
13 decreases with plastic strain because of the increase in dislocation density. Nevertheless, for
14 body-centered cubic (bcc) metals, dislocations must overcome Peierls-Nabarro barriers (*i.e.*,
15 Peierls internal stress), such that the thermal activation area is not related with strain. Hence,
16 the yield stress of fcc metals is determined mainly by strain hardening, but that of bcc metals
17 is basically determined by strain rate hardening and temperature softening. Based on these
18 considerations, they proposed the Zerilli-Armstrong (ZA) model with different constitutive
19 forms for fcc, bcc and hexagonal close-packed (hcp) metals which owns mixed
20 characteristics of the bcc and fcc structures. However, Voyiadjis and Abed (2005a) pointed
21 out in the Voyiadjis-Abed (VA) model that the ZA model is not applicable to the deformation
22 of metals under high temperature and that this model does not include the strain rate effect on
23 thermal activation area., then they proposed the modified ZA model as an improvement
24 (Abed and Voyiadjis, 2005). Nemat-Nasser et al. (1998, 1999) introduced a varying reference
25 strain rate, as a function of strain and temperature, and developed the Nemat-Nasser-Li (NNL)
26 model, applicable to both fcc and bcc metals. Follansbee and Kocks (1988) developed a
27 constitutive model for polycrystalline copper using a concept of mechanical threshold stress
28
29
30
31
32
33
34
35
36
37
38
39
40
41
42
43
44
45
46
47
48
49
50
51
52
53
54
55
56
57
58
59
60
61
62
63
64
65

1 (MTS), the flow stress at 0 K representing the structural evolution of the material. However,
2
3 this model needs various experimental data and phenomenologically-based expressions to
4
5 determine the thermal component of MTS which cannot be explicitly expressed directly,
6
7 leading to a complex constitutive form which is hard to use. Gao and Zhang (2010) proposed
8
9 a Gao-Zhang (GZ) model for fcc metals which considered the microstructural evolution by
10
11 using the internal state variable MTS. Based on the consistent dislocation analysis, they
12
13 further developed a new constitutive model for hcp metals (2011) considering that hcp metals
14
15 own partial structural characteristics of both bcc and fcc metals. In addition, Langer et al.
16
17 (2010) presented a Langer-Bouchbinder-Lookman (LBL) model based on the thermodynamic
18
19 theory of dislocation-mediated plasticity, which differs from conventional
20
21 dislocation-mediated continuum theories by introducing equations of motion for the flow of
22
23 energy and entropy associated with dislocations using an ‘effective’ temperature.
24
25
26
27
28
29
30
31
32

33
34 However, the models mentioned above are generally suitable for the conventional strain
35
36 rate range below $10^4 s^{-1}$ and do not apply if the strain rate is extremely high, say beyond
37
38 $10^4 s^{-1}$. Follansbee and Kocks (1988) found experimentally that the flow stress of oxygen-free
39
40 high conductivity (OFHC) copper and some other fcc metals increases dramatically when
41
42 strain rate exceeds a critical value. Fig.1 shows the dependence of the flow stress of OFHC
43
44 copper on the strain rate and compares the predictions of these conventional models with
45
46 experimental results. Obviously, these conventional models all are not capable of reflecting
47
48 what the experiment shows. A rapid upturn of flow stress occurs when the strain rate
49
50 approaches $10^4 s^{-1}$ (the critical strain rate for the beginning of upturn is located within a
51
52 transition zone of $[10^{3.6}, 10^4] s^{-1}$ as shown in Fig. 1). Correspondingly, there also appears a
53
54
55
56
57
58
59
60
61
62
63
64
65

1 continuous fast rise in the strain rate sensitivity. It is worth recalling that strain rate sensitivity
2
3
4 is an important hardening index defined by $m_s = \frac{\partial(\log\sigma)}{\partial(\log\dot{\epsilon})}\bigg|_{T,\epsilon}$, where σ is the true stress,
5
6
7 $\dot{\epsilon}$ is the plastic strain rate, ϵ denotes plastic strain and T is the absolute temperature. The
8
9
10 strain rate sensitivity under extremely high strain rates observed in experiment is much higher
11
12
13 than those predicted by the constitutive models mentioned above. Considering that the
14
15
16 parameters in these models were determined by the experimental data at relatively low strain
17
18
19 rates, we have attempted to determine them again using the high-strain-rate experimental data.
20
21
22 Unfortunately, we confirmed that these models updated are still unable to correctly reflect the
23
24
25 experimental results under high strain rates. The strain rate sensitivities built in these models
26
27
28 do not seem to have captured the actual deformation mechanisms in the metals under an
29
30
31 extremely high strain rate.

32
33 Follansbee and Kocks (1988) pointed out that the plastic deformation under a very high
34
35
36 strain rate of $10^4 s^{-1}$ is still controlled by the thermally activated dislocation mechanism, and
37
38
39 that the postulated transition mechanism of rate-controlled deformation from thermal
40
41
42 activation control to dislocation drag control does not occur at high strain rates. Although
43
44
45 Rusinek et al (2010) showed in their Modified Rusinek-Klepaczko (MRK) model that both
46
47
48 thermally activated and viscous drag mechanisms are operative within high strain rate range,
49
50
51 Zerilli and Armstrong (1992) proved that dislocation drag is not the reason for the strong
52
53
54 upturn of the flow stress as demonstrated in Fig. 1, because the uniform strain in a tension
55
56
57 test should increase at high strain rates, but the dislocation-drag model concludes the opposite.
58
59
60 This indicates that when the strain rate is beyond a critical value, something unclear in the
61
62
63 thermal activation mechanism must have played a key role. For instance, an enhanced growth
64
65

1 rate of dislocation generation (or enhanced accumulation rate of dislocations) will become
2
3 dominant when strain rate approaches $10^4 s^{-1}$ (Clough et al., 2003). To explain the upturn
4
5 phenomenon, Follansbee and Kocks introduced empirically a new factor to their model – the
6
7 effect of strain rate on the initial strain hardening rate. They considered that the observed
8
9 change in the strain rate sensitivity was due to the strain rate sensitivity of the structure
10
11 evolution. Nemat-Nasser and Li (1998) included the effect of the enhanced dislocation
12
13 accumulation rate by redefining the mean dislocation spacing and dislocation density. In this
14
15 way, however, the modified term was only defined as the function of temperature and strain,
16
17 but not the strain rate. Molinari and Ravichandran (2005) tried to simulate the upturn by
18
19 introducing the characteristic length evolution of a material's microstructure. As a matter of
20
21 fact, all the above investigations converge to the same conclusion, i.e., when the strain rate
22
23 approaches $10^4 s^{-1}$, the growth rate of dislocation generation begins to accelerate, leading to
24
25 an abrupt increase of dislocation density and a rapid decrease of the dislocation characteristic
26
27 lengths (e.g., dislocation spacing, activation area, cell size, etc.), and in turn, inducing an
28
29 upturn of the flow stress. Hence, we can conclude that the dislocation density evolution
30
31 (DDE), which characterizes the structure evolution, must be considered in a constitutive
32
33 model for describing the deformation of a metal under very high strain rates.
34
35
36
37
38
39
40
41
42
43
44
45
46

47 Klepaczko and Chiem (1986) pointed out that in fcc metals (e.g., copper and aluminium),
48
49 the rate sensitivity of strain hardening plays an important role. They then proposed a general
50
51 relationship for structural evolution using the DDE with generation and annihilation terms.
52
53 Subsequently, Klepaczko (1991) presented a consistent approach for microstructure-related
54
55 constitutive modelling of the rate- and temperature-dependent plasticity of metals based on
56
57
58
59
60
61
62
63
64
65

1 DDE. Kubin and Estrin (1990) proposed a pair of coupled differential equations to describe
2
3 the evolution of the densities of mobile and forest dislocations with strain. However, their
4
5 equations can only be solved by a numerical method if the initial values of the dislocation
6
7 densities and the four material constants are known (Chinh et al., 2004). Ma et al. (2004)
8
9 developed a dislocation density based constitutive model for fcc single crystals at elevated
10
11 temperatures but at low strain rates. Voyiadjis and Abed (2005b) considered the effect of
12
13 DDE on the thermomechanical response of metals with different crystal structures in their
14
15 new VA model. Voyiadjis and Almasri (2008) included the evolution of mobile dislocation
16
17 density of fcc metals in the Voyiadjis-Almasri (VAI) model by adding a term of mobile
18
19 dislocation density rate into the traditional relationship of strain rate and dislocation velocity.
20
21 Wei et al. (2008) investigated the strain hardening of fcc metals by using the Kocks-Mecking
22
23 (KM) and Estrin-Mecking (EM) evolution equations of single structure parameter (i.e., total
24
25 dislocation density). Based on the evolutions of mobile and immobile dislocation densities,
26
27 Austin and McDowell (2011) also presented a dislocation-based constitutive model for
28
29 viscoplastic deformation of fcc metals at very high strain rates. However, this model was
30
31 intended to address the deformation of polycrystalline fcc metals with micro-scale grains
32
33 subjected to shock waves and especially to describe the flow response on the plastic wave
34
35 front (the shock stress amplitude is a few tens of GPa). There is still some other literature
36
37 involving the discussion of mobile dislocation density (e.g. Kameda and Zikry, 1998; Roters,
38
39 2003; Wang et al., 2008; Roters et al., 2010).
40
41
42
43
44
45
46
47
48
49
50
51
52
53
54
55
56
57
58
59
60
61
62
63
64
65

1 Although quite some models have been proposed based on DDE, the physics of the
2
3 dislocation generation at extremely high strain rates is still not very clear. In this paper, we
4
5 will investigate the evolution of mobile dislocation density and incorporate it into our
6
7 previously established constitutive model for fcc metals to develop a new model, so as to
8
9 explain the flow-stress upturn phenomenon at extremely high strain rates. Section 2 of the
10
11 paper will describe how to develop the new constitutive model based on the theory of DDE
12
13 and thermal-activation rate-control analysis. Section 3 will explain the determination of the
14
15 constitutive parameters for OFHC copper, and Section 4 will compare the model with
16
17 experimental data for validation and provide the model's predictions within a wide range of
18
19 strain rates and temperature.
20
21
22
23
24
25
26
27
28
29
30

31 **2. Constitutive modelling**

32
33 The plastic deformation of metals can be regarded as the process of dislocation motion
34
35 and accumulation under the rate-controlled deformation mechanism. In the thermal activation
36
37 analysis, plastic flow is mainly controlled by the motion of dislocations which is opposed by
38
39 both short- and long-range obstacles. The former may be overcome by thermal activation,
40
41 whereas the latter are essentially independent of the temperature (or in other words, athermal).
42
43 The short-range barriers may include forest dislocations (mainly in fcc metals), Peierls stress
44
45 (mainly in bcc metals), point defects (e.g., vacancies and self-interstitials), alloy elements,
46
47 solute atoms (interstitials and substitutionals), impurities, deposits and so on. The long-range
48
49 barriers may include grain boundaries, far-field dislocation forests and other microstructural
50
51 elements with far-field influence (Nemat-Nasser and Li, 1998). Therefore, the flow stress of
52
53
54
55
56
57
58
59
60
61
62
63
64
65

the materials, which is defined by the material resistance to dislocation motion, can be decomposed as

$$\sigma = \sigma_{ath} + \sigma_{th} \quad (1)$$

where σ_{ath} is the athermal component of flow stress, reflecting mainly the long-range barriers; and σ_{th} is the thermal component of flow stress, reflecting mainly the short-range barriers. Similarly, the MTS (denoted as $\hat{\sigma}$) can be decomposed as $\hat{\sigma} = \hat{\sigma}_{ath} + \hat{\sigma}_{th}$. Then the flow stress of the material can be expressed as the following since the MTS is regarded as a structure parameter,

$$\sigma = \hat{\sigma}_{ath} + f(\dot{\epsilon}, T) \cdot \hat{\sigma}_{th} \quad (2)$$

where $f(\dot{\epsilon}, T)$ (< 1.0) represents the strain rate and temperature effects in thermal activation. In the following subsections, we will establish a new constitutive model for fcc metals under extremely high strain rates to remove the barrier in the previous GZ model (2010) which is applicable only when the strain rate is below $10^4/s$.

2.1. Thermal stress

2.1.1. The microstructure evolution characterized by mobile dislocation density

For the dislocation structure in a deformed material, it can be assumed that the mean total dislocation-density (ρ) can be additively decomposed into two components (Shia and Zikry, 2009): $\rho = \rho_i + \rho_m$, where ρ_i is the immobile dislocation density and ρ_m is the mobile dislocation density. The DDE is always defined using the monotonously varying plastic strain, which is a satisfactory choice as an independent state variable to describe the structural evolution. During the continuously increasing strain history, dislocations emerge and

annihilate. The general balance equation to account for dislocation generation, interaction, trapping and recovery is (Klepaczko and Chiem, 1986):

$$d\rho/d\varepsilon = M_{eff}(\rho, \dot{\varepsilon}, T) = M_g(\rho, \dot{\varepsilon}) - M_a(\rho, \dot{\varepsilon}, T) \quad (3)$$

where M_{eff} is the effective obstacle multiplication coefficient, M_g corresponds to the generation of defects (dislocations) and M_a is the contribution of dynamic recovery via rate and temperature-dependent dislocation annihilation and rearrangement. Eq. (3) is the general law which describes the strain-induced evolution of the material microstructure based on the accumulation and recovery of dislocations.

In most constitutive models involving DDE, the mobile dislocation density is not separately studied because at a relatively low strain rate, the mobile dislocation density is small in comparison to the immobile dislocation density and is approximately considered as a constant. In so doing, the total dislocation density acts as a single structural parameter. At an extremely high strain rate, however, the evolution of the mobile dislocation density should receive a specific consideration in the thermal stress for fcc metals. In reality it is difficult to determine the evolution law of the mobile dislocation density because the mobile dislocation density cannot be discerned directly under transmission electron microscopy (TEM), and hence some indirect methods, such as the kinetic relation analysis or ultrasonics, have to be used (Klepaczko, 1991). Thus in this study, we determine the evolution equation of mobile dislocation density by the following approximation. Wang et al. (2008) concluded that the mobile dislocation density would be the main part in the total dislocation density when the deformation was at extremely high strain rates, i.e., $\rho \approx \rho_m$. Besides, as presented in (Voyiadjis and Abed, 2005b), the mobile dislocation density could be related to the total

1 dislocation density by a linear relation, $\rho_m = f\rho$ ($f < 1.0$), where f could change with
 2
 3 ρ , but a constant value always gives satisfactory quantitative results for most metals. This
 4
 5 linear relation may be verified too by the evolution curves of the total dislocation density and
 6
 7 mobile dislocation density (Ma and Roters, 2004). Actually, the assumption that the total and
 8
 9 mobile dislocation densities are approximately equal had been used for the Orowan's
 10
 11 equation in the deduction of the Haasen constitutive model (Moosbrugger, 1995). Based on
 12
 13 the investigations above, we can reasonably use the evolution equation of the total dislocation
 14
 15 density as a good approximation of the mobile dislocation density.
 16
 17
 18
 19
 20
 21

22 There are many proposed DDE equations as discussed previously. The most used is the
 23
 24 Klepaczko model (Klepaczko and Chiem, 1986), which, when applying to the mobile
 25
 26 dislocation density, gives rise to
 27
 28
 29

$$30 \frac{\partial \rho_m}{\partial \varepsilon} = M_{II}(\dot{\varepsilon}) - k_a(\dot{\varepsilon}, T)(\rho_m - \rho_{m0}) \quad (4)$$

31 where $M_{II}(\dot{\varepsilon})$ is the initial multiplication rate of mobile dislocations, $k_a(\dot{\varepsilon}, T)$ is the
 32
 33 dynamic recovery coefficient. Eq. (4) will become identical to the well-known evolution
 34
 35 equation of Kubin and Estrin (1990) when the forest dislocation density is relatively
 36
 37 considered as constant at very high strain rates, indicating that Eq. (4) is quite reliable.
 38
 39
 40
 41
 42
 43
 44
 45

46 In the above equation, M_{II} is proportional to the strain hardening rate θ_{II} which
 47
 48 reflects dislocation accumulation (i.e., $M_{II} \sim \theta_{II}$). At the same time, there is $\theta_{II} \sim \log \dot{\varepsilon}$ for
 49
 50 copper by experiments (Follansbee and Kocks, 1988). So, Klepaczko (1991) proposed
 51
 52

$$53 M_{II}(\dot{\varepsilon}) = M_0[1 + \tanh(c_0 X)], \quad X = \log(\dot{\varepsilon} / \dot{\varepsilon}_{s0}) \quad (5)$$

54 where M_0 and c_0 are constants, and $\dot{\varepsilon}_{s0}$ is the saturated reference strain rate.
 55
 56
 57
 58
 59

60 On the other hand, $k_a(\dot{\varepsilon}, T)$ was also proposed by Klepaczko for fcc metals as
 61
 62
 63
 64
 65

$$k_a(\dot{\varepsilon}, T) = k_0(\dot{\varepsilon} / \dot{\varepsilon}_{s0})^{-c_1 T} \quad (6)$$

where k_0 is the annihilation factor at $T=0$, and c_1 is the absolute rate sensitivity due to defect annihilation related to the parameters characterizing cross-slip.

By integrating Eq. (4), we get

$$\rho_m = \rho_m(\varepsilon, \dot{\varepsilon}, T) = \rho_{m0} + \frac{M_0}{k_0} \left\{ 1 + \tanh \left[c_0 \log \left(\frac{\dot{\varepsilon}}{\dot{\varepsilon}_{s0}} \right) \right] \right\} \cdot \left(\frac{\dot{\varepsilon}}{\dot{\varepsilon}_{s0}} \right)^{c_1 T} \cdot \left\{ 1 - \exp \left[-k_0 \left(\frac{\dot{\varepsilon}}{\dot{\varepsilon}_{s0}} \right)^{-c_1 T} \cdot \varepsilon \right] \right\} \quad (7)$$

As we have known, the deformation of a metal is the result of the movement of mobile dislocations whose speed depends on strain rate and density varies with strain. In the process of deformation, the increase of the total dislocation density makes the plastic flow of the material easier, which eventually softens the material. At the same time, however, the possibility of dislocation interactions also increases, which lowers down the percentage of the dislocation density in the total and makes the plastic flow difficult. Therefore, the evolution of the total dislocation density cannot directly explain the deformation behavior of a metal. It should be the mobile dislocation density that actually contributes to the deformation under extremely high strain rates. Austin and McDowell (2011) also confirmed that models which distinguished the mobile and immobile components of dislocation density will provide a better description of microstructure evolution in plastic deformation.

2.1.2. Formulating the thermal stress

As discussed in our previous model, the thermal stress can be expressed as

$$\sigma_{th} = \hat{\sigma}_{th} \cdot \left\{ 1 - [-c_2 T \ln(\dot{\varepsilon} / \dot{\varepsilon}_0)]^{1/q} \right\}^{1/p} \quad (8)$$

where $c_2 = k/(g_0\mu b^3)$ (k is the Boltzmann constant, g_0 is nominal activation energy, μ is the shear modulus of material, and b is Burgers vector). The thermal component of MTS, $\hat{\sigma}_{th}$, standing for the threshold of the thermal stress, is related with the material's microstructure as well as its evolution. As suggested by Zerilli and Armstrong (1987) and Voyiadjis and Abed (2005a), it follows the relation:

$$\hat{\sigma}_{th} \sim mG_0 / A_0b \quad (9)$$

where m is the orientation factor ($\sigma = m\tau$), $G_0 = g_0\mu b^3$ is the reference free energy of thermal activation at 0 K, A_0 is the dislocation activation area at $T=0$. The actual activation area, A , is a measure of the mean distance between mobile dislocations, l_m , by the following relationship

$$A \sim l_m b \quad (10)$$

while the effective mobile dislocation density is related with the mobile dislocation spacing by

$$\rho_m \sim l_m^{-2} \quad (11)$$

Presuming that the couple of Eqs. (10) and (11) can be approximately employed to determine A_0 in Eq. (9) (Zerilli and Armstrong, 1987), then:

$$\hat{\sigma}_{th} = C\sqrt{\rho_m} \quad (12)$$

where $C = mG_0 / b^2$. This expression can be verified too in the literature (Shia and Zikry, 2009; Mecking and Kocks, 1981).

By combining Eqs. (7), (8) and (12) and neglecting the initial mobile dislocation density which is much less than the values during large deformation (Wang et al., 2008), we finally get the thermal stress:

$$\sigma_{th} = \hat{C} \cdot \sqrt{\left\{ 1 + \tanh \left[c_0 \log \left(\frac{\dot{\epsilon}}{\dot{\epsilon}_{s0}} \right) \right] \right\} \cdot \left(\frac{\dot{\epsilon}}{\dot{\epsilon}_{s0}} \right)^{c_1 T} \cdot \left\{ 1 - \exp \left[-k_0 \left(\frac{\dot{\epsilon}}{\dot{\epsilon}_{s0}} \right)^{-c_1 T} \epsilon \right] \right\}} \cdot \left\{ 1 - \left[-c_2 T \ln \left(\frac{\dot{\epsilon}}{\dot{\epsilon}_0} \right) \right]^{1/q} \right\}^{1/p} \quad (13)$$

where $\hat{C} = C\sqrt{M_0/k_0}$ which is the reference thermal stress.

2.2. Athermal stress

2.2.1. The athermal stress based on microstructure identification

In our previous constitutive model as well as in the ZA model for fcc metals, the athermal stress was defined as:

$$\sigma_{ath} = \sigma_G + \sigma_S = \sigma_G + k_S d^{-1/2} \quad (14)$$

where σ_G is the stress due to initial defects, σ_S is the stress induced by the size effect (e.g., grain-size), d is the diameter of the grain and k_S is a microstructural constant. The grain-size stress can be regarded as a constant for a given material if there is no physical change (e.g., twinning) to alter the mean grain size during plastic deformation. However, deformation twinning may take place in the plastic deformation of fcc metals at very high strain rates or within an ultrafine-grain and a nano-crystal. Twinning subdivides the grains and therefore increases the barriers to slip, and hence the work-hardening rate. Twinning has a much lower sensitivity to strain rate and temperature. So the contribution of twinning to flow stress should be incorporated into the athermal stress, which should not alter the thermal stress. It has been pointed out by Meyers et al. (2001) and Beyerlein and Tomé (2008) that in most cases the grain-size stress with twinning still obeys a Hall-Petch (HP) relationship, but

with a slope k_r that is higher than k_s for slip. In other words, $\sigma_s = k_T d^{-1/2}$ ($k_T > k_s$).

Such greater dependence of the twinning stress on grain size, in comparison with the slip stress, is a very unique characteristic of twinning, as pointed out by Armstrong and Worthington (1973).

In reality, the HP relationship has been experimentally shown to apply to the relationship of material's strength and twin spacing (λ , the mean spacing between adjacent twin boundaries) (Meyers and Chawla, 1999). Klepaczko (1991) also concluded that the effect of the twin spacing on the internal stress in polycrystalline metals and alloys follows the same relationship as that of the grain size (d). Shen et al. (2005) presented a strengthening mechanism of twin boundary (TB) analogous to that of grain boundary (GB) in nano-crystalline metals. Thus, the stress component due to the size effect can be expressed as

$$\sigma_s = k_d d^{-1/2} + k_\lambda \lambda^{-1/2} \quad (15)$$

where k_d and k_λ are constants of slopes respectively.

2.2.2. Microstructure evolution in athermal stress

In fcc metals, the athermal stress also undergoes a microstructure evolution during the process of plastic deformation, which has been neglected in most models. The HP relationship of the reciprocal of activation volume and the grain size has been observed to describe the size effect, which can be rationalized by combining the dislocation pile-up model and the thermal activation analysis of plastic flow rate. Considering the similar role of TB and GB (both are effective in strengthening the material by blocking dislocation motions), a

generalized HP relationship for the reciprocal of activation volume can be written as (Lu et al., 2009)

$$(V^{-1} - V_0^{-1}) = k_d d^{-1/2} + k_\lambda \lambda^{-1/2} \quad (16)$$

where V is the apparent activation volume measured in experiments and V_0 is the physical activation volume associated with the intra-grain or intra-twin dislocation mechanism, i.e. intersection of lattice dislocations. $k_d = k_d(V_{GB})$ and $k_\lambda = k_\lambda(V_{TB})$ where V_{GB} and V_{TB} are the activation volumes associated with the GB- and TB-mediated mechanism, respectively. Setting $\tilde{V}^{-1} = (V^{-1} - V_0^{-1})$, then using $\tilde{V} \sim \tilde{l} b^2 / 2$ and $\tilde{\rho} \sim \tilde{l}^{-2}$ (where \tilde{l} is an ‘equivalent’ mean distance between the dislocations interacted with long-range obstacles in the far field, and $\tilde{\rho}$ is the corresponding dislocation density), there is

$$(V^{-1} - V_0^{-1}) \sim \sqrt{\tilde{\rho} - \tilde{\rho}_0} \quad (17)$$

As the far-field dislocations generally contain various dislocation sources, the evolution equation of the far-field dislocation density cannot be obtained directly. However, considering that the athermal stress is basically independent of the strain rate and temperature and relies mainly on strain (Klepaczko et al., 1985), we can adopt a simplified form of Eq. (4) for the far-field dislocation density, in which the parameters $M_{II}(\dot{\epsilon})$ and $k_a(\dot{\epsilon}, T)$ are no longer related with strain rate and temperature but constants M_{II0} and k_{a0} (Klepaczko, 1991).

Hence,

$$\tilde{\rho} = \tilde{\rho}_0 + \lambda_a [1 - \exp(-k_{a0} \epsilon)] \quad (18)$$

where $\lambda_a = \bar{f} (M_{II0} / k_{a0})$, and \bar{f} is a constant additionally introduced to denote the fraction of long-range dislocation in the total dislocation as suggested by Voyiadjis and Abed (2005b). By combining Eqs. (15), (16), (17) and (18), we get

$$\sigma_S = B[1 - \exp(-k_{a0}\varepsilon)]^{1/2} \quad (19)$$

where $B = m\alpha\mu b\sqrt{\lambda_a}$ (α is an empirical coefficient often taken to be 0.2 for fcc metals).

So, the athermal stress is finally

$$\sigma_{ath} = \sigma_G + B[1 - \exp(-k_{a0}\varepsilon)]^{1/2} \quad (20)$$

The function in the right hand side of Eq. (19) could be fitted by a power-law function which is always used as an approximate description of the athermal stress (Chinh et al., 2004). However, Eq. (19) is more precise in essence because it can reflect the final saturation state of strain hardening. In addition, the expression for the athermal stress in Eq. (20) will remain the same form whether there appears deformation twinning or not, provided that the parameters are determined by corresponding data. Compared with the thermal component of the flow stress, the size effect of twinning is relatively limited in fcc metals unless the twin spacing approaches to several hundred nanometers or less.

2.3. Flow stress

Finally, by combining Eqs. (13) and (20), we obtain the following new constitutive relation for the flow stress of fcc metals at extremely high strain rates:

$$\sigma_f = \sigma_{ath} + \sigma_{th} = \sigma_G + B[1 - \exp(-k_{a0}\varepsilon)]^{1/2} + \hat{C} \cdot \sqrt{1 - \exp\left[-k_0\left(\frac{\dot{\varepsilon}}{\dot{\varepsilon}_{s0}}\right)^{-c_1T} \varepsilon\right]} \cdot \sqrt{\left\{1 + \tanh\left[c_0 \log\left(\frac{\dot{\varepsilon}}{\dot{\varepsilon}_{s0}}\right)\right]\right\} \cdot \left(\frac{\dot{\varepsilon}}{\dot{\varepsilon}_{s0}}\right)^{c_1T} \cdot \left\{1 - \left[-c_2T \ln\left(\frac{\dot{\varepsilon}}{\dot{\varepsilon}_0}\right)\right]^{1/q}\right\}^{1/p}} \quad (21)$$

In the new model, the constant parameters to be determined are (σ_G, B, k_{a0}) for the athermal part and $(\hat{C}, k_0, c_0, c_1, c_2, p, q, \dot{\varepsilon}_{s0}, \dot{\varepsilon}_0)$ for the thermal part.

The above one-dimensional constitutive equation can be easily extended to three dimensional (3D) descriptions by relating the true stress and plastic strain with the Mises equivalent stress and equivalent plastic strain of stress/strain tensors. For isotropic hardening, the von Mises yielding criterion is:

$$f = \frac{3}{2} \mathbf{S} : \mathbf{S} - \sigma_y^2(\bar{\varepsilon}^p, \dot{\varepsilon}^p, T) = 0 \quad (22)$$

where $\bar{\sigma} = \sqrt{\frac{3}{2} \mathbf{S} : \mathbf{S}}$ is defined as the equivalent stress ($\mathbf{S} = \boldsymbol{\sigma} - \frac{\sigma_{kk}}{3} \mathbf{I}$ is the deviatoric stress); σ_y is the yield stress defined by a constitutive description such as the model of Eq.

(21); $\bar{\varepsilon}^p$ is the equivalent plastic strain defined by $\bar{\varepsilon}^p = \int \dot{\bar{\varepsilon}}^p dt = \int \sqrt{\frac{2}{3} \dot{\boldsymbol{\varepsilon}}^p : \dot{\boldsymbol{\varepsilon}}^p} dt$. The 3D

constitutive form can then be directly integrated with a finite element code for material dynamic calculations (such as high speed machining where the deformation rate of materials is always beyond $10^4 s^{-1}$). A framework for numerical integration of crystal elasto-plastic constitutive equations compatible with explicit finite element codes is available in (Kuchnicki et al., 2006; Amirkhizi and Nemat-Nasser, 2007; Li et al., 2008; Rossiter et al., 2010). In addition, the anisotropic yield function and hardening behavior of fcc crystalline plasticity was discussed elsewhere (e.g. Hana et al., 2003; Abedrabbo et al., 2007; Wang et al., 2009; Khan and Baig, 2011).

During the plastic deformation process, the majority of the plastic work will be converted to internal dissipation heat in materials, i.e., $Q_{int} = \eta W^P$, where η is the converting coefficient (also called the Taylor-Quinney empirical constant, generally ranging between 0.9 and 1.0 at high deformation rate). If the adiabatic shear phenomenon appears at high strain

1 rates, the heat will result in a rapid increase of temperature within the local zone of adiabatic
 2
 3 shear band (ASB). The real temperature can be calculated by
 4

$$5 \quad T = T_0 + \frac{\eta}{\rho_M c_p} \int_0^{\varepsilon^P} \sigma d\varepsilon^P \quad (23)$$

6
 7
 8
 9
 10 where T_0 is the initial temperature, ρ_M is the material's density, c_p is the material's
 11
 12 specific heat at constant pressure. So the state variable of temperature must be updated
 13
 14 continuously at each strain increment in the flow stress calculation under the case of an
 15
 16 adiabatic process. In addition, dynamic strain aging (DSA) which induces a local rise
 17
 18 phenomenon in the stress-temperature curve appears mainly at low strain rates. At high strain
 19
 20 rates, it may exist only for alloys. Its effect is local and limited and will not be considered
 21
 22 here.
 23
 24
 25
 26
 27
 28
 29
 30
 31

32 *2.4. A unified constitutive model*

33
 34
 35 It is not easy to develop a single equation applicable to both the conventional strain rate
 36
 37 range (from $10^{-4} s^{-1}$ to $10^4 s^{-1}$) and the extremely high strain rate range (from $10^4 s^{-1}$ to
 38
 39 $10^6 s^{-1}$, considering that the strain rate on the wave front of strong shock is about
 40
 41 $10^7 - 10^9 s^{-1}$). Most of the existing thermo-viscoplastic constitutive models of metallic
 42
 43 materials cannot fulfill the requirement. This is the case even for the MRK model which
 44
 45 adopted a mixed form of combining the dislocation-slip mechanism with the dislocation-drag
 46
 47 mechanism. As we know, the PTW model has a piecewise constitutive form so as to patch
 48
 49 together low-rate and extremely-high-rate regime in a phenomenological way. In light of this
 50
 51 precedent, it is feasible in practice to acquire a unified equation based on the new model we
 52
 53 established above.
 54
 55
 56
 57
 58
 59
 60
 61
 62
 63
 64
 65

We know from the discussion in previous sections that our new model could well describe the dynamics deformation behavior at a relatively high strain rate ($\varepsilon > \varepsilon^{cr}$). We note that the new model can be simplified for the case of relatively low strain rates ($\varepsilon < \varepsilon^{cr}$). This can be done based on the assumption that at below the critical strain rate, the strain rate effect on the evolution of mobile dislocation density in the thermal stress becomes negligible. Hence, the evolution equation of Eq. (4) can be reduced to a simple form by treating $M_H(\dot{\varepsilon})$ and $k_a(\dot{\varepsilon}, T)$ as constants. Furthermore, it is generally unnecessary to consider strain hardening in the athermal stress for fcc metals. Thus, by setting $k_{a0} = 0$, $c_0 = 0$ and $c_1 = 0$ in Eq. (21), we obtained the simplified form of our new model, Eq. (21), for deformation under $\varepsilon < \varepsilon^{cr}$, i.e.,

$$\sigma_f = \sigma_G + \hat{C} \cdot \sqrt{1 - \exp(-k_0 \varepsilon)} \cdot \left\{ 1 - \left[-c_2 T \ln \left(\frac{\dot{\varepsilon}}{\dot{\varepsilon}_0} \right) \right]^{1/q} \right\}^{1/p} \quad (24)$$

Hence, we could propose a unified constitutive model in the form of a piecewise function as

$$\sigma_f = \begin{cases} \text{Expression of Eq. (21),} & \text{when } \varepsilon > \varepsilon^{cr} \\ \text{Expression of Eq. (24),} & \text{when } \varepsilon < \varepsilon^{cr} \end{cases} \quad (25)$$

3. Parameter determination for OFHC copper

In the following, we will determine the material parameters of the constitutive model for a typical fcc metal, the fully-annealed polycrystalline OFHC copper of high purity (>0.9999).

The framework of our parameter determining method has been introduced in our previous work (2011).

1 Firstly, we will determine the parameters in the athermal stress which is uncoupled with
 2 the thermal stress and has a simple functional form. Based on the experimental stress-strain
 3 curve of OFHC Copper at temperature (>1000 K) (Nemat-Nasser and Li, 1998), the three
 4 parameters in the athermal stress can be determined by nonlinear curve fitting as:

$$11 \quad \sigma_G = 52 \text{ MPa} , B = 230 \text{ MPa} , k_{a0} = 0.64$$

14 Secondly, we noticed that parameters $\dot{\epsilon}_0$ and $\dot{\epsilon}_{s0}$ are included in the logarithmic
 15 function and thus the influence of their changes is very small relative to c_1 and c_2 . Besides,
 16 they are dependent on c_1 and c_2 respectively. Hence, if $\dot{\epsilon}_0$ and $\dot{\epsilon}_{s0}$ can be evaluated in
 17 advance, most errors in the evaluation can be offset by the subsequent numerical fitting of c_1
 18 and c_2 . In this way, we not only avoid the problem caused by their diverse values reported in
 19 the literature, but also enhance the robustness of the algorithm of determining other
 20 parameters. Based on the above consideration, let us take $\dot{\epsilon}_0 = 1.76 \times 10^8 \text{ s}^{-1}$ obtained from
 21 the VA model of OFHC copper, and $\dot{\epsilon}_{s0} = 3.75 \times 10^{10} \text{ s}^{-1}$ according to the ZA model of
 22 OFHC copper.

23 The remaining seven parameters, $(\hat{C}, k_0, c_0, c_1, c_2, p, q)$, can be determined based on the
 24 experimental data of OFHC copper at high strain rates by Follansbee and Kocks (1988).
 25 There are several ways to obtain them. For example, they can be obtained by curve fitting
 26 individually. In this way, however, the parameter values cannot be optimal, because the
 27 individual determination does not count for the influence of the others to minimize the
 28 discrete error of the experimental data. The finite element analysis has also been used to
 29 determine these parameters numerically, but needs significant computational effort. Grediac
 30 and Pierron (2005) attempted to use the virtual fields method (VFM) to identify the

1 constitutive parameters of an elasto-plastic equation when the full-field kinematic
2
3 measurements were available at the surface of the test specimens. However, the applicability
4
5 of this method to visco-plastic equations has not yet been established. To overcome these
6
7 problems, a constrained nonlinear multi-variable optimization method developed by us (2011)
8
9 was adopted to obtain the optimal parameters as a whole. As we have pointed out, there are
10
11 two types of the multi-variable optimization methods. The local algorithm (LA) converges
12
13 quickly but depends strongly on the initial values of variables, resulting in the risk of not
14
15 obtaining a globally optimal solution. The global algorithm (GA) is insensitive to the initial
16
17 values of variables but needs a vast computational resource and may be not determinate at the
18
19 end to obtain a solution. Our optimization approach combines the genetic method of GA and
20
21 the interior-point penalty function method of LA, by first carrying out the GA with a
22
23 moderate calculating scale to obtain a group of preliminarily optimized results, and then
24
25 using the LA to obtain the final optimized results with these preliminarily optimized results
26
27 as the initial values of the variables. A matlab program has been developed to carry out the
28
29 above optimization procedure. Moreover, the physically reasonable ranges of these
30
31 parameters, which are necessary in optimization as a set of inequality constraints, are
32
33 theoretically evaluated below:
34
35
36
37
38
39
40
41
42
43
44
45

46
47 (i) Ranges of k_0 and c_0
48
49

50 At conventional strain rates, the strain hardening relation is approximate $\sqrt{\varepsilon}$ in OFHC
51
52 copper (Zerilli and Armstrong, 1987). So in Eq. (7), there is $k_0 \approx (\dot{\varepsilon} / \dot{\varepsilon}_{s0})^{c_1 T}$ if using the
53
54 approximation of Taylor progression of exponent function. Its maximum value can be
55
56 estimated as 1.0, and the theoretically evaluated range of k_0 may be taken as [1, 10]
57
58
59
60
61
62
63
64
65

1 considering that its value should become greater at very high strain rates. In addition, the
 2
 3 maximum value of c_0 included in M_H can be calculated as 0.9 by the approximate relation
 4
 5 of $M_H(\dot{\epsilon}) \sim \dot{\epsilon}$ (Klepaczko, 1991). Hence, c_0 is assumed to be within [0.1, 1].
 6
 7

8
 9 *(ii) Ranges of c_1 and c_2*

10
 11 In the definition of $c_2 = k/(g_0\mu b^3)$, the Boltzmann constant $k = 1.3806505 \times 10^{-23}$ J/K,
 12
 13 the shear modulus $\mu = E/2(1+\nu) = 48$ GPa and the Burgers vector $b = 2 \times 10^{-10}$ m have
 14
 15 been known for copper. The only unknown constant is the nominal activation energy g_0 . But
 16
 17 it has been known that the range of g_0 is [0.2, 2] for medium strength of a single obstacle of
 18
 19 barriers in dislocation motion (Frost and Ashby, 1982). Then we can obtain the theoretically
 20
 21 evaluated range of c_2 is $[1.8 \times 10^{-5}, 1.8 \times 10^{-4}]$. The range of c_1 is of the same order of
 22
 23
 24
 25
 26
 27
 28
 29 c_2 .

30
 31 *(iii) Ranges of p and q*

32
 33 As we know, (p, q) is a pair of parameters representing the potential shape of barriers
 34
 35 in a crystal. According to the physical nature of the barrier, there is $p \in (0, 1]$ and $q \in [1, 2]$
 36
 37 for a single crystal structure (Kocks et al., 1975). Some typical cases of the (p, q) pair are:
 38
 39 (2/3, 1) for a rectangular barrier, (1/2, 2) for a hyperbolic barrier and (1, 2) for a sinusoidal
 40
 41 barrier. The other commonly used values of (2/3, 1), (2/3, 2), (3/4, 4/3) and (1, 1) in the
 42
 43 literature can all be considered as the transitional state between the rectangular shape and the
 44
 45 sinusoid shape.
 46
 47
 48
 49
 50

51
 52 In addition, the value of parameter \hat{C} is equal to 808 MPa in the GZ model for the
 53
 54 conventional strain rate range. If using this value as a reference, its range can be estimated as
 55
 56 [1000, 10000] MPa since the threshold of thermal stress will be larger at higher strain rates.
 57
 58
 59
 60
 61
 62
 63
 64
 65

1 Finally, we can obtain the optimized results for the constitutive parameters in the new model
2
3 of Eq. (21) as shown in Table 1(a). At the same time, we can use the identical approach
4
5 introduced above to determine the constitutive parameters in the reduced model of Eq. (24)
6
7 based on the experimental data of copper at relatively low strain rates by Follansbee and
8
9 Kocks (1988). The results are shown in Table 1(b).
10
11
12
13
14
15
16

17 **4. Model validation and prediction**

18
19 In this section, all the model predictions of flow stress are adiabatic, and so the
20
21 temperatures indicated in the following figures are only initial temperatures.
22
23
24

25 Fig. 2 compares the predictions of the new unified model with those of the others,
26
27 together with the relevant experimental data, on the flow stress variation with strain rate in
28
29 annealed OFHC copper at room temperature and at a given strain of 0.15. It is worth noting
30
31 that the pioneering measurements of plasticity at extremely high strain rates are rare (Swegle
32
33 and Grady, 1985; Huang and Clifton, 1985; Follansbee and Kocks, 1988; Tong et al., 1992),
34
35 and are not all consistent (probably due to different experimental conditions). When
36
37 comparing our model predictions with the measurements of Huang and Clifton as well as
38
39 Tong et al., we found that the new model gives very good predictions ($\sim 5\%$ error in
40
41 average), indicating that our model is very capable in reconciling the deformation behavior of
42
43 the material at extremely high strain rates. When compared with the data of Follansbee and
44
45 Kocks as fitted by the MTS model, the new model is greater by 15% error at around $10^4 s^{-1}$,
46
47 while the reduced model has a good agreement in the low-rate range. The MRK and VAI
48
49 models adjacent to the new model present similar rate sensitivities, while the prediction of the
50
51
52
53
54
55
56
57
58
59
60
61
62
63
64
65

1 Armstrong-Arnold-Zerilli (AAZ) model (2007) does not cope with the presented
2 measurements, because this model is only a simple power-law fitting of the limited data
3 points of Swegle and Grady which is too higher than the other experimental data shown here.
4
5

6
7
8
9 In Fig. 3, the new model and other models' predictions of stress-strain curves were
10 compared with Clifton's test data at a strain rate of $6.4 \times 10^5 s^{-1}$. It is seen that compared
11 with other conventional models, our new model can well describe the flow stress-strain
12 behavior of OFHC copper at such a high strain rate. This is understandable because our
13 model (as well as the MTS model) has developed the thermal threshold stress to reflect the
14 abrupt rise of rate sensitivity at extremely high strain rates. We noticed that there is a gap
15 between the MTS model prediction and Clifton's data. The reason for this is that the flow
16 stress magnitude of Kocks' experimental data is essentially lower than that of Clifton's data.
17
18
19
20
21
22
23
24
25
26
27
28
29
30

31 As the Clifton's primary data of copper were obtained by pressure-shear impact test, an
32 orientation factor (m) should be applied to convert the resolved shear stress and plastic shear
33 strain to the axial flow stress and axial plastic strain. As we know, in the plastic deformation
34 of crystals there exist different slip systems in grains; so the orientation factor of a material is
35 defined as the mean reciprocal Schmid factor by using the statistically averaging principle
36 over all possible grain orientations. For single crystals, the orientation factor is equal to $\frac{\sqrt{3}}$
37 based on the macroscopic phenomenological plastic yielding criterion for the onset of
38 plasticity (Zhang, 2001). For polycrystals, there are two approaches mostly used in the
39 analysis of texture formation of metallic plastic deformation, i.e., the Taylor model ($m = 3.07$)
40 and the Sachs model ($m = 2.24$). Also there are some intermediate models used to predict the
41 texture transition and stress-strain behavior of polycrystals at large viscoplastic deformation,
42
43
44
45
46
47
48
49
50
51
52
53
54
55
56
57
58
59
60
61
62
63
64
65

1 which are built up by combining the two classic models with a weight factor between 0
2
3 (Taylor model) and 1.0 (Sachs model). So, the orientation factor as an empirical value
4
5 actually varies within a range [2.24, 3.07] due to different crystalline texture formation
6
7
8
9 during the plastic deformation processes of materials (Soppa et al., 1998).

10
11 However, the Sachs model, which assumes identical stresses in grains and one active slip
12
13 system in each grain, is generally applied for low and intermediate strain (Carstensen and
14
15 Pedersen, 1997), while the Taylor model, which assumes identical strain in all grains of the
16
17 polycrystal and multi-slip systems in a grain, is more suitable for large plastic deformation at
18
19 high strain rates (Frost and Ashby, 1982). Therefore the Taylor factor $m = 3.07$ is adopted
20
21 here in Figs. 2 and 3 for Clifton's data of copper which deforms at extremely high strain rates.
22
23
24
25 The flow stress magnitude predicted by the new model based on the Clifton's data with
26
27 Taylor factor is in agreement with the experimental results of 8000 s^{-1} by Nemat-Nasser
28
29 and Li (1998). This verifies the applicability of the Taylor's factor here.

30
31
32
33
34
35
36
37 Fig. 4 gives the predictions of flow stress versus strain under very high strain rates at
38
39 room and elevated temperatures. The curve of $6.4 \times 10^5 \text{ s}^{-1}$ which has been verified above by
40
41 experimental data is replotted here as a reference. It is noticed that the stress-strain curve
42
43 becomes almost flat when the strain exceeds a certain value, indicating that strain hardening
44
45 tends towards the saturation state. In reality, at conventional strain rates the saturation of
46
47 strain hardening happens late at relatively larger strain, then the power-law expression can be
48
49 used as an approximate description of strain hardening in general but it cannot describe the
50
51 saturation state in itself. At very high strain rates the strain hardening will saturate earlier at
52
53 strains less than 0.3. The flow stress will approach the maximal saturation value at first and
54
55
56
57
58
59
60
61
62
63
64
65

1 then begins to gradually descend. The reason for this is that the thermal softening effect due
2
3 to adiabatic shear, which is quite obvious at very high strain rates, becomes enough to reach a
4
5 balance with the strain hardening effect and will further exceed it with the increase of strain.
6
7 This strain hardening behaviour can be well predicted by the present model owing to the new
8
9 exponential expressions for strain hardening in the thermal and athermal components of the
10
11 flow stress.
12
13
14
15
16

17 Fig. 5 shows the dependence of the thermal stress on temperature in OFHC copper at
18
19 $1.0 \times 10^5 \text{ s}^{-1}$ and different strains, which quantitatively reflects the thermal softening effect on
20
21 the flow stress in thermal activation mechanism of plastic deformation. It can be found that
22
23 the thermal stress decreases quickly with temperature especially at low temperature. The
24
25 thermal softening effect is more distinct at a large strain, and the softening processes are
26
27 almost the same when the strain is greater than 0.30. It is obvious that the thermal component
28
29 of flow stress will eventually disappear at a critical temperature $T^{cr} = [-(k/G_0) \ln(\dot{\epsilon}/\dot{\epsilon}_0)]^{-1}$
30
31 because the thermal activation decreases with the rise of temperature until its minimum zero
32
33 value but the value cannot be negative. This means that the flow stress approaches to its
34
35 athermal component with the rise of temperature and eventually becomes independent of
36
37 temperature at a critical temperature where the barriers of dislocation cease to be important.
38
39 Thus, the thermal stress should be removed from the constitutive model if $T > T^{cr}$, and only
40
41 the athermal stress remains finally. In addition, Nemat-Nasser and Li (1998) provided a more
42
43 complete formula of calculating the critical temperature in their model, in which the critical
44
45 temperature will depend on the plastic strain too besides strain rate, but it is not easy to be
46
47 solved due to its implicit form.
48
49
50
51
52
53
54
55
56
57
58
59
60
61
62
63
64
65

5. Conclusions

This paper has carried out an investigation into the fcc crystalline plasticity under an extremely high strain rate beyond $10^4 s^{-1}$, where the strain rate sensitivity becomes high. A new dislocation-mechanics-based constitutive model has been developed. Compared to our previous fcc model as well as to the other classic fcc models, the present model incorporates the evolution of mobile dislocation density, which is established based on the balance law of dislocation formation, to describe the microstructural evolution of the material. At the same time, a unified constitutive model is proposed by investigating the reduced form of the new model to cover both the low and high strain rate ranges.

In the application of the new model to OFHC copper, the model parameters were determined by an optimization method composed of a global genetic algorithm and a local penalty-function algorithm so as to obtain globally optimal parameters within their theoretically evaluated ranges. The flow stress predictions of the unified model proposed have shown good agreements with most of the experimental data of OFHC copper in the strain rate range from $10^{-4} s^{-1}$ to $6.4 \times 10^5 s^{-1}$. The flow stress upturn phenomenon in OFHC copper is satisfactorily described.

Acknowledgments

This research work was supported by the Australian Research Council and by the Project of the National Natural Science Foundation of China (No. 50877070) and the Open

1 Foundation of State Key Laboratory of Explosion Science and Technology of China (No.
2
3 KFJJ11-9Y).
4
5

6 7 8 9 **References**

10
11
12
13
14
15
16
17
18
19
20
21
22
23
24
25
26
27
28
29
30
31
32
33
34
35
36
37
38
39
40
41
42
43
44
45
46
47
48
49
50
51
52
53
54
55
56
57
58
59
60
61
62
63
64
65

Abed, F.H., Voyiadjis, G.Z., 2005. A consistent modified Zerilli-Armstrong flow stress model for BCC and FCC metals for elevated temperatures. *Acta Mech.* 175, 1-18.

Abedrabbo, N., Pourboghrat, F., Carsley, J., 2007. Forming of AA5182-O and AA5754-O at elevated temperatures using coupled thermo-mechanical finite element models. *Int. J. Plasticity* 23, 841-875.

Amirkhizi, A.V., Nemat-Nasser, S., 2007. A framework for numerical integration of crystal elasto-plastic constitutive equations compatible with explicit finite element codes. *Int. J. Plasticity* 23, 1918-1937.

Armstrong, R.W., Worthington, P.J., 1973. In: *Metallurgical Effects at High Strain Rates*. New York: Plenum Press.

Armstrong, R.W., Arnold, W., Zerilli, F.J., 2007. Dislocation Mechanics of Shock-Induced Plasticity, *Metall. Mater. Trans. A* 38A, 2605-2610.

Arsecularatne, J.A., Zhang, L.C., 2004. Assessment of constitutive equations used in machining. *Key Eng. Mater.* 274, 277-282.

Austin, R.A., McDowell, D.L., 2011. A dislocation-based constitutive model for viscoplastic deformation of fcc metals at very high strain rates. *Int. J. Plasticity* 27, 1-24.

Beyerlein, I.J., Tomé, C.N., 2008. A dislocation-based constitutive law for pure Zr including temperature effects. *Int. J. Plasticity* 24, 867-895.

- 1 Carstensen, J.V., Pedersen, O.B., 1997. Texture and grain-size effects on cyclic plasticity in
2
3 copper and copper-zinc. *Mater. Sci. Eng. A* 234-236, 497-500.
4
5
6 Chaboche, J.L., 2008. A review of some plasticity and viscoplasticity constitutive theories.
7
8
9 *Int. J. Plasticity* 24, 1642-1693.
10
11
12 Chinh, N.Q., Horvath, G., Horita, Z., Langdon, T.G., 2004. A new constitutive relationship
13
14 for the homogeneous deformation of metals over a wide range of strain. *Acta Mater.* 52,
15
16 3555-3563.
17
18
19 Clough, R.B., Webb, S.C., Armstrong, R.W., 2003. Dynamic hardness measurements using a
20
21 dropped ball: with application to 1018steel. *Mater. Sci. Eng. A* 360, 396-407.
22
23
24
25 Frost, H.J., Ashby, M.F., 1982. *Deformation Mechanism Maps*. Oxford: Pergamon Press.
26
27
28 Follansbee, P.S., Kocks, U.F., 1988. A constitutive description of the deformation of copper
29
30 based on the use of mechanical threshold stress as an internal state variable. *Acta Metall.*
31
32 36, 81-93.
33
34
35
36 Gao, C.Y., Zhang, L.C., 2010. A constitutive model for dynamic plasticity of FCC metals.
37
38
39 *Mater. Sci. Eng. A* 527, 3138-3143.
40
41
42 Gao, C.Y., Zhang, L.C., Yan, H.X., 2011. A new constitutive model for HCP metals. *Mater.*
43
44 *Sci. Eng. A* 528, 4445-4452.
45
46
47 Grediac, M., Pierron, F., 2005. Applying the Virtual Fields Method to the identification of
48
49 elasto-plastic constitutive parameters. *Int. J. Plasticity* 22, 602-627.
50
51
52
53 Hana, C.S., Chung, K., Wagoner, R.H., Oh, S.I., 2003. A multiplicative finite elasto-plastic
54
55 formulation with anisotropic yield functions. *Int. J. Plasticity* 19, 197-211.
56
57
58
59
60
61
62
63
64
65

- 1 Huang, S., Clifton, R.J., 1985. In: Kawata K, Shioiki J (eds.). Macro and Micro-Mechanics of
2
3 High Velocity Deformation and Fracture, IUTAM. Tokyo, pp.63.
4
5
6 Johnson, G., Cook, W., 1985. Fracture characteristics of three metals subjected to various
7
8 strain, strain rates, temperature and pressures. Eng. Fract. Mech. 21, 31-48.
9
10
11 Kameda, T., Zikry, M.A., 1998. Three dimensional dislocation-based crystalline constitutive
12
13 formulation for ordered intermetallics. Scripta Mater. 38(4), 631-636.
14
15
16 Khan, A.S., Huang, S., 1992. Experimental and theoretical study of mechanical behavior of
17
18 1100 aluminum in the strain rate range 10^{-5} - 10^4 s⁻¹. Int. J. Plasticity 8, 397-424.
19
20
21 Khan A.S., Liang, R.Q., 1999. Behaviors of three BCC metal over a wide range of strain rates
22
23 and temperatures: experiments and modelling. Int. J. Plasticity 15, 1089-1109.
24
25
26 Khan, A.S., Suh, Y.S., Kazmi, R., 2004. Quasi-static and dynamic loading responses and
27
28 constitutive modelling of titanium alloys. Int. J. Plasticity 20, 2233-2248.
29
30
31 Khan, A.S., Baig, M., 2011. Anisotropic responses, constitutive modeling and the effects of
32
33 strain-rate and temperature on the formability of an aluminum alloy. Int. J. Plasticity 27,
34
35 522-538.
36
37
38 Klepaczko, J.R., Rouxel, A., Chiem, C.Y., 1985. Proc. Cong. Int. DYMAT 85 (Editions de
39
40 Physique), C5-57.
41
42 Klepaczko, J.R., Chiem, C.Y., 1986. On rate sensitivity of f.c.c. metals, instantaneous rate
43
44 sensitivity and rate sensitivity of strain hardening. J. Mech. Phys. Solids 34, 29-54.
45
46
47 Klepaczko, J.R., 1991. Physical-state variables - the key to constitutive modelling in dynamic
48
49 plasticity. Nucl. Eng. Des. 127, 103-115.
50
51
52
53
54
55
56
57
58
59
60
61
62
63
64
65

- 1 Kocks, U.F., Argon, A.S., Ashby, M.F., 1975. Thermodynamics and kinetics of slip. In:
2
3 Progress in Materials Science (Chapt 19). Pergamon Press.
4
5
6 Kubin, L.P., Estrin, Y., 1990. Evolution of dislocation densities and the critical conditions for
7
8 the Portevin-Lechatelier effect. *Acta Metall. Mater.* 38(5), 697-708.
9
10
11 Kuchnicki, S.N., Cuitino, A.M., Radovitzky, R.A., 2006. Efficient and robust constitutive
12
13 integrators for single-crystal plasticity modeling. *Int. J. Plasticity* 22, 1988-2011.
14
15
16 Langer, J.S., Bouchbinder, E., Lookman, T., 2010. Thermodynamic theory of dislocation-
17
18 mediated plasticity. *Acta Mater.* 58, 3718-3732.
19
20
21 Li, H.W., Yang H., Sun, Z.C., 2008. A robust integration algorithm for implementing rate
22
23 dependent crystal plasticity into explicit finite element method. *Int. J. Plasticity* 24,
24
25 267-288.
26
27
28
29 Lin, Y.C., Chen, X.M., 2011. A critical review of experimental results and constitutive
30
31 descriptions for metals and alloys in hot working. *Mater. Des.* 32, 1733-1759.
32
33
34 Lu, L., Dao, M., Zhu, T., Li, J., 2009. Size dependence of rate-controlling deformation
35
36 mechanisms in nanotwinned copper. *Scripta Mater.* 60, 1062-1066.
37
38
39
40 Ma, A., Roters, F., 2004. A constitutive model for fcc single crystals based on dislocation
41
42 densities and its application to uniaxial compression of aluminium single crystals. *Acta*
43
44 *Mater.* 52, 3603-3612.
45
46
47
48 Mecking, H. , Kocks, U.F., 1981. Kinetics of flow strain-hardening. *Acta Metall.* 29(11),
49
50 1865-1875.
51
52
53
54
55 Meyers, M. A., 1994. *Dynamic behavior of materials.* John Wiley & Sons., New York.
56
57
58
59 Meyers, M.A., Chawla, K.K., 1999. *Mechanical Behavior of Materials.* Prentice Hall.
60
61
62
63
64
65

- 1 Meyers, M.A., Vohringer, O., Lubarda, V.A., 2001. The Onset of Twinning: A Constitutive
2
3 Description. *Acta Mater.* 49, 4025-4039.
4
5
6 Molinari, A., Ravichandran, G., 2005. Constitutive modelling of high-strain-rate deformation
7
8 in metals based on the evolution of an effective microstructural length. *Mech. Mater.* 37,
9
10 737-752.
11
12
13
14 Moosbrugger, J.C., 1995. Continuum slip viscoplasticity with the Haasen constitutive model:
15
16 application to CdTe single crystal inelasticity. *Int. J. Plasticity* 11(7), 799-826.
17
18
19
20 Nemat-Nasser, S., Li, Y.L., 1998. Flow stress of FCC polycrystals with application to OFHC
21
22 Cu. *Acta Mater.* 46, 565-577.
23
24
25 Nemat-Nasser, S., Guo, W., Cheng, J., 1999. Mechanical properties and deformation
26
27 mechanisms of a commercially pure titanium. *Acta Mater.* 47, 3705-3720.
28
29
30
31 Preston, D.L., Tonks, D.L., Wallace, D.C., 2003. Model of plastic deformation for extreme
32
33 loading conditions. *J. Appl. Phys.* 93, 211-220.
34
35
36
37 Remington, B.A., et al., 2006. Material dynamics under extreme conditions of pressure and
38
39 strain rate. *Mater. Sci. Tech.* 22, 474-488.
40
41
42 Rossiter, J., Brahme A., Simha, M.H., Inal, K., Mishra, R., 2010. A new crystal plasticity
43
44 scheme for explicit time integration codes to simulate deformation in 3D microstructures:
45
46 Effects of strain path, strain rate and thermal softening on localized deformation in the
47
48 aluminum alloy 5754 during simple shear. *Int. J. Plasticity* 26, 1702-1725.
49
50
51
52
53 Roters, F., 2003. A new concept for the calculation of the mobile dislocation density in
54
55 constitutive models of strain hardening. *Phys. Stat. Sol. (b)* 240(1), 68-74.
56
57
58
59
60
61
62
63
64
65

- 1 Roters, F., Eisenlohr, P., Hantcherli, L., Tjahjanto, D.D., Bieler, T.R., Raabe, D., 2010.
2
3 Overview of constitutive laws, kinematics, homogenization and multiscale methods in
4 crystal plasticity finite-element modelling: Theory, experiments, applications. *Acta*
5
6 *Mater.* 58, 1152-1211.
7
8
9
10
11 Rusinek, A., Rodriguez-Martinez, J.A., Arias, A., 2010. A thermo-viscoplastic constitutive
12 model for FCC metals with application to OFHC copper. *Int. J. Mech. Sci.* 52, 120-135.
13
14
15
16
17 Shia, J., Zikry, M.A., 2009. Grain-boundary interactions and orientation effects on crack
18 behaviour in polycrystalline aggregates. *Int. J. Solids Struct.* 46(21), 3914-3925.
19
20
21
22
23 Shen, Y.F., Lu, L., Lu, Q.H., Jin, Z.H., Lu, K., 2005. Tensile properties of copper with
24 nano-scale twins. *Scripta Mater.* 52, 989-994.
25
26
27
28 Soppa, E., Amos, D., Schmauder, S., Bischo, E., 1998. The influence of second phase and/or
29 grain orientations on deformation patterns in a Ag polycrystal and in Ag/Ni composites.
30
31 *Comput. Mater. Sci.* 13, 168-176.
32
33
34
35
36 Steinberg, D.J. , Cochran, S.G. , Guinan M.W., 1980. A constitutive model for metals
37 applicable at high rate. *J. Appl. Phys.* 51, 1498~1504.
38
39
40
41
42 Steinberg, D.J., Lund, C.M., 1989. A constitutive model for strain rates from 10^4 to 10^6 s⁻¹. *J.*
43 *Appl. Phys.* 65, 1528-1533.
44
45
46
47 Sung, J.H., Kim, J.H., Wagoner, R.H., 2010. A plastic constitutive equation incorporating
48 strain, strain-rate, and temperature. *Int. J. Plasticity* 26, 1746-1771.
49
50
51
52
53 Swegle, J.W., Grady, D.E., 1985. Shock viscosity and the prediction of shock wave rise times,
54
55
56 *J. Appl. Phys.* 58, 692-701.
57
58
59
60
61
62
63
64
65

- 1 Tong, W., Clifton, R.J., Huang, S.H., 1992. Pressure-shear impact investigation of strain rate
2
3 history effects in oxygen-free high-conductivity copper. *J. Mech. Phys. Solids* 40(6),
4
5 1251-1294.
6
7
8
9 Voyiadjis, G.Z., Abed, F.H., 2005a. Microstructural based models for BCC and FCC metals
10
11 with temperature and strain rate dependency. *Mech. Mater.* 37, 355-378.
12
13
14 Voyiadjis, G.Z., Abed, F.H., 2005b. Effect of dislocation density evolution on the
15
16 thermomechanical response of metals with different crystal structures at low and high
17
18 strain rates and temperatures. *Archives Mech.* 57, 299-343.
19
20
21
22 Voyiadjis, G.Z., Almasri, A.H., 2008. A physically based constitutive model for fcc metals
23
24 with applications to dynamic hardness. *Mech. Mater.* 40, 549-563.
25
26
27
28 Wang, Z.Q., Beyerlein, I.J., LeSar, R., 2008. Slip band formation and mobile dislocation
29
30 density generation in high rate deformation of single fcc crystals. *Phil. Magazine* 88(9),
31
32 1321-1343.
33
34
35
36 Wang, Z.Q., Beyerlein, I.J., LeSar, R., 2009. Plastic anisotropy in fcc single crystals in high
37
38 rate deformation. *Int. J. Plasticity* 25, 26-48.
39
40
41
42 Wei, W., Wei, K.X., Fan, G.J., 2008. A new constitutive equation for strain hardening and
43
44 softening of fcc metals during severe plastic deformation. *Acta Mater.* 56, 4771-4779.
45
46
47 Zerilli, F.J., Armstrong, R.W., 1987. Dislocation-mechanics-based constitutive relations for
48
49 material dynamics calculation. *J. Appl. Phys.* 5, 1816-1825.
50
51
52
53 Zerilli, F.J., Armstrong, R.W., 1992. The effect of dislocation drag on the stress-strain
54
55 behavior of f.c.c. metals. *Acta Metall. Mater.* 40(8), 1803-1808.
56
57
58
59 Zhang, L.C., 2001. *Solid Mechanics for Engineers*, New York: Palgrave.
60
61
62
63
64
65

List of Tables:

Table 1 Final optimized results of the constitutive parameters of OFHC copper

(a) For the new model of Eq. (21)

(b) For the reduced model of Eq. (24)

List of Figure Captions:

Fig 1 Comparison of some conventional models' predictions with experimental data (Follansbee and Kocks, 1988) for the dependence of the flow stress on strain rate in annealed OFHC copper at a strain of 0.15.

Fig. 2 Comparison of the new unified model's predictions with experimental data and other models for the dependence of the flow stress on strain rate in annealed OFHC copper at room temperature and a strain of 0.15.

Fig. 3 Comparison of different model predictions with Clifton's experimental data (Follansbee and Kocks, 1988) for the relation of flow stress versus strain in annealed OFHC copper at $6.4 \times 10^5 s^{-1}$ and room temperature.

Fig. 4 Model predictions of the relations of flow stress versus strain for OFHC Copper under very high strain rates at room and elevated temperatures.

Fig. 5 Dependence of the thermal stress on temperature for OFHC Copper at $1.0 \times 10^5 s^{-1}$ and different strains.

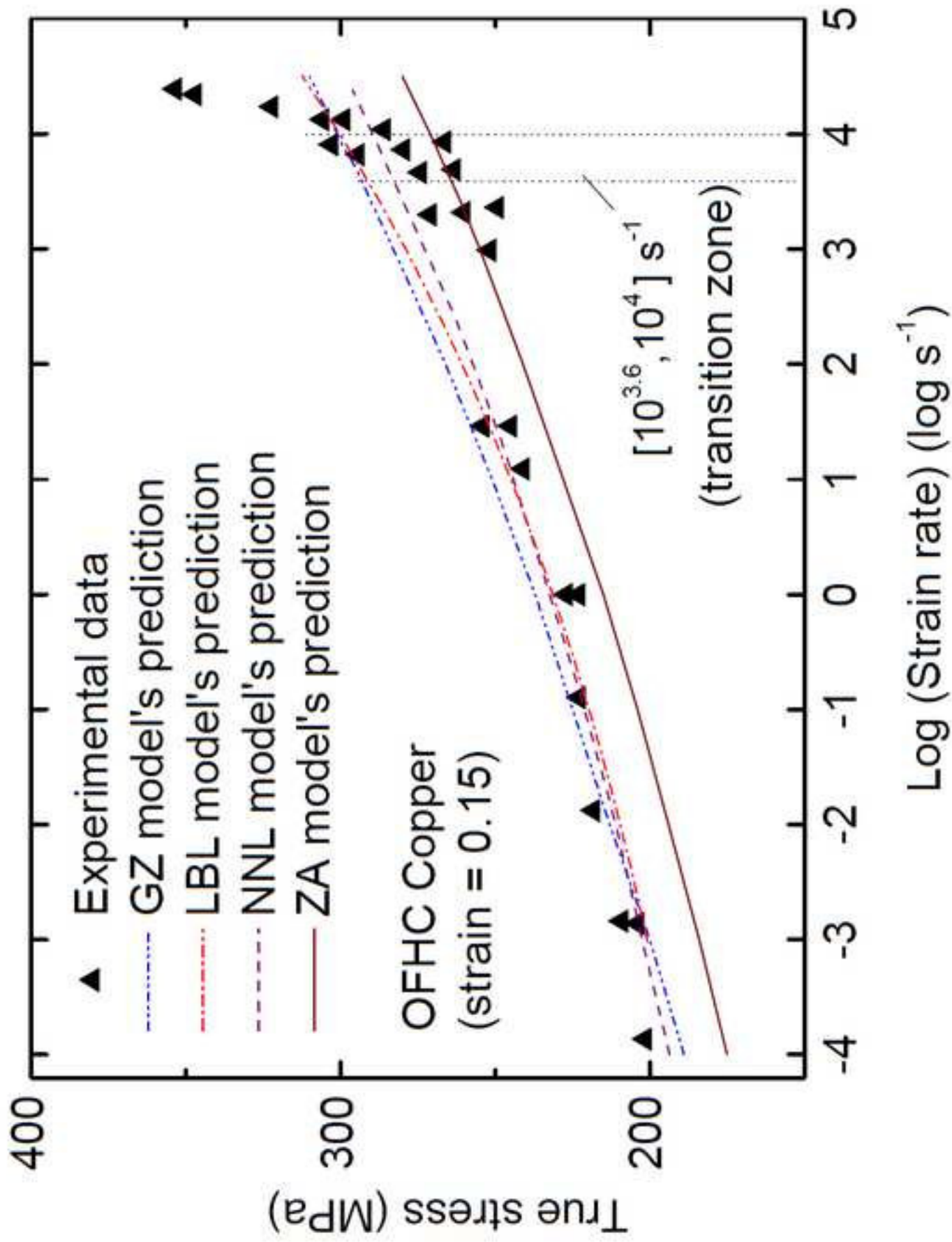


Figure 1

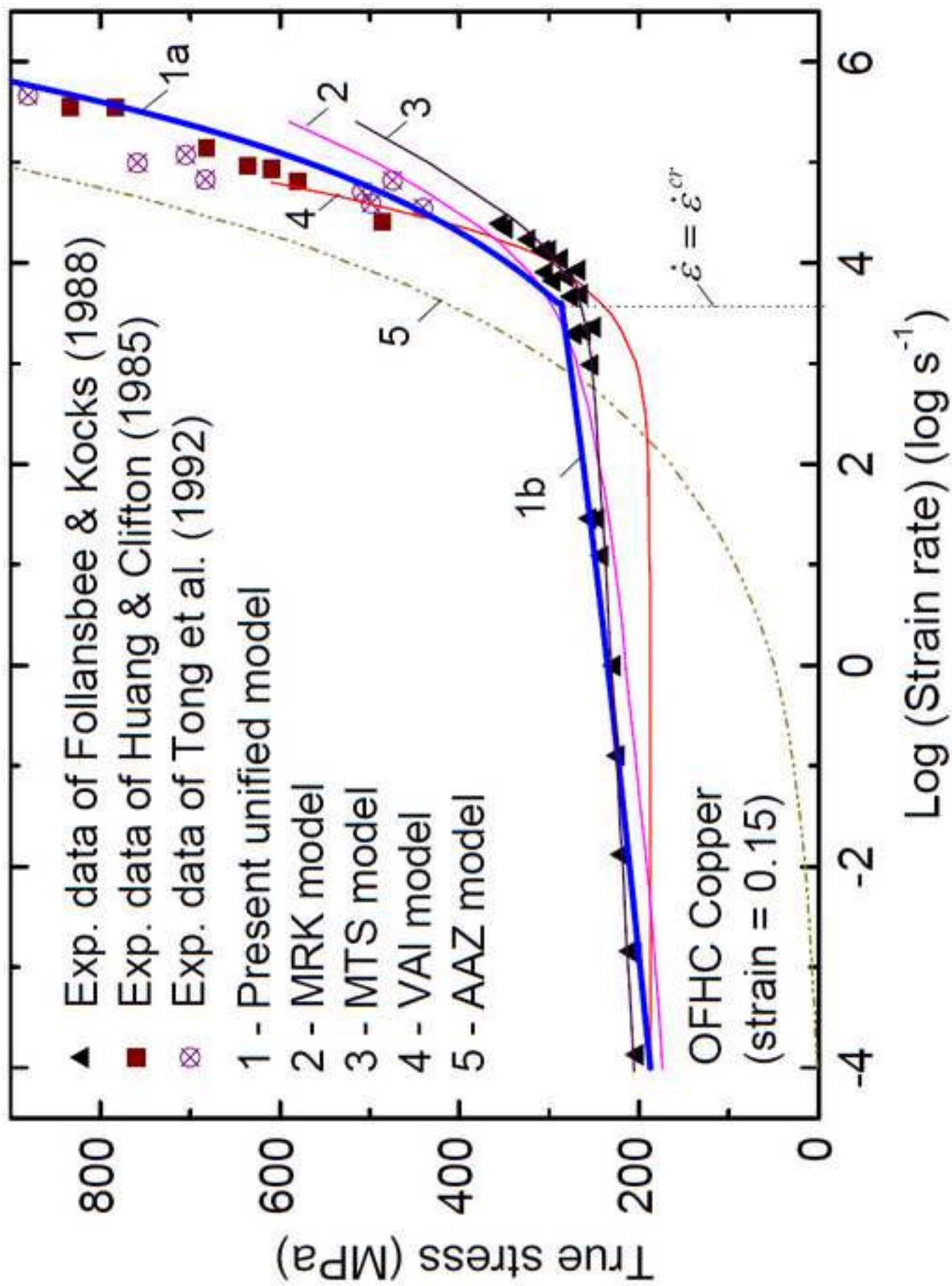


Figure 2

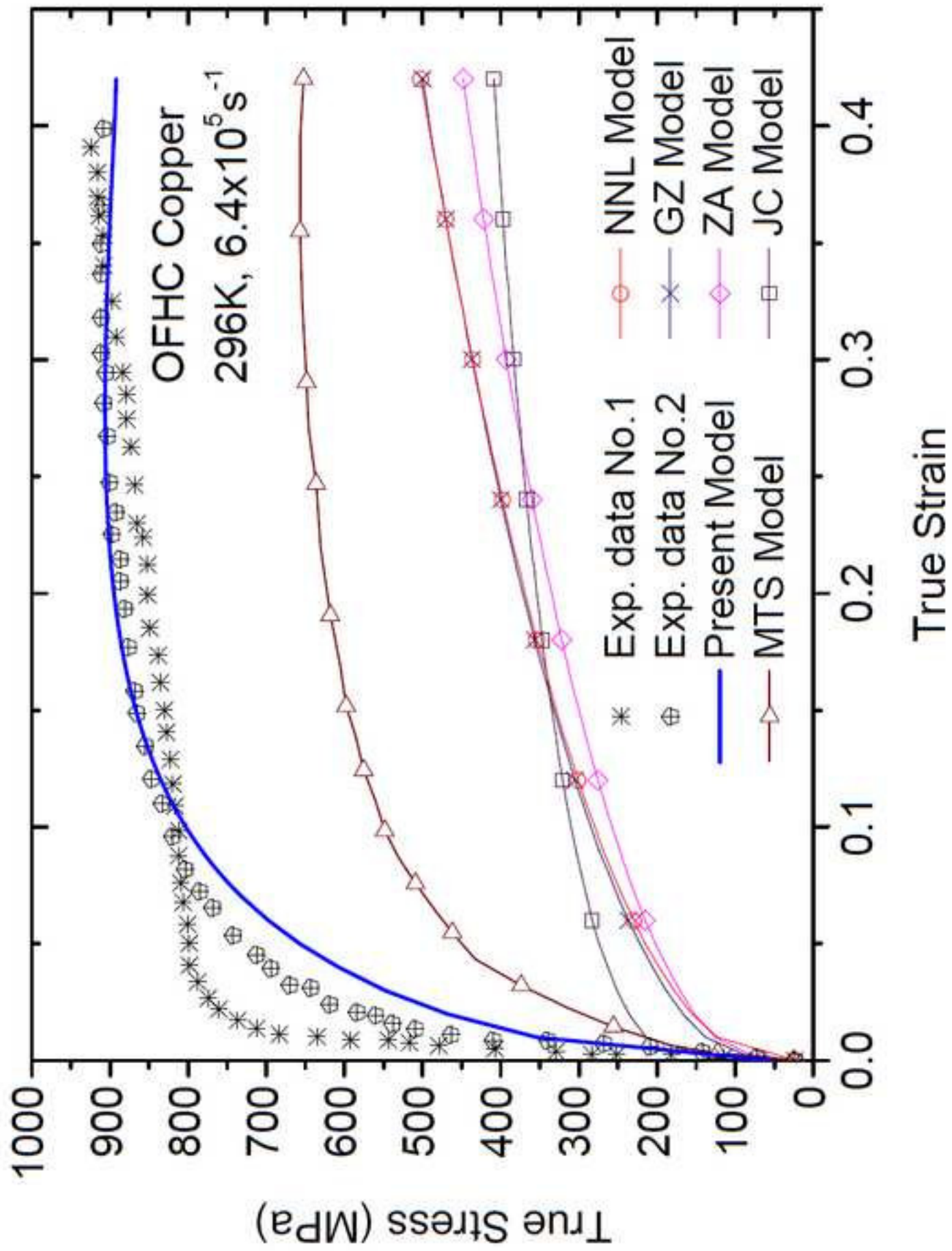


Figure 3

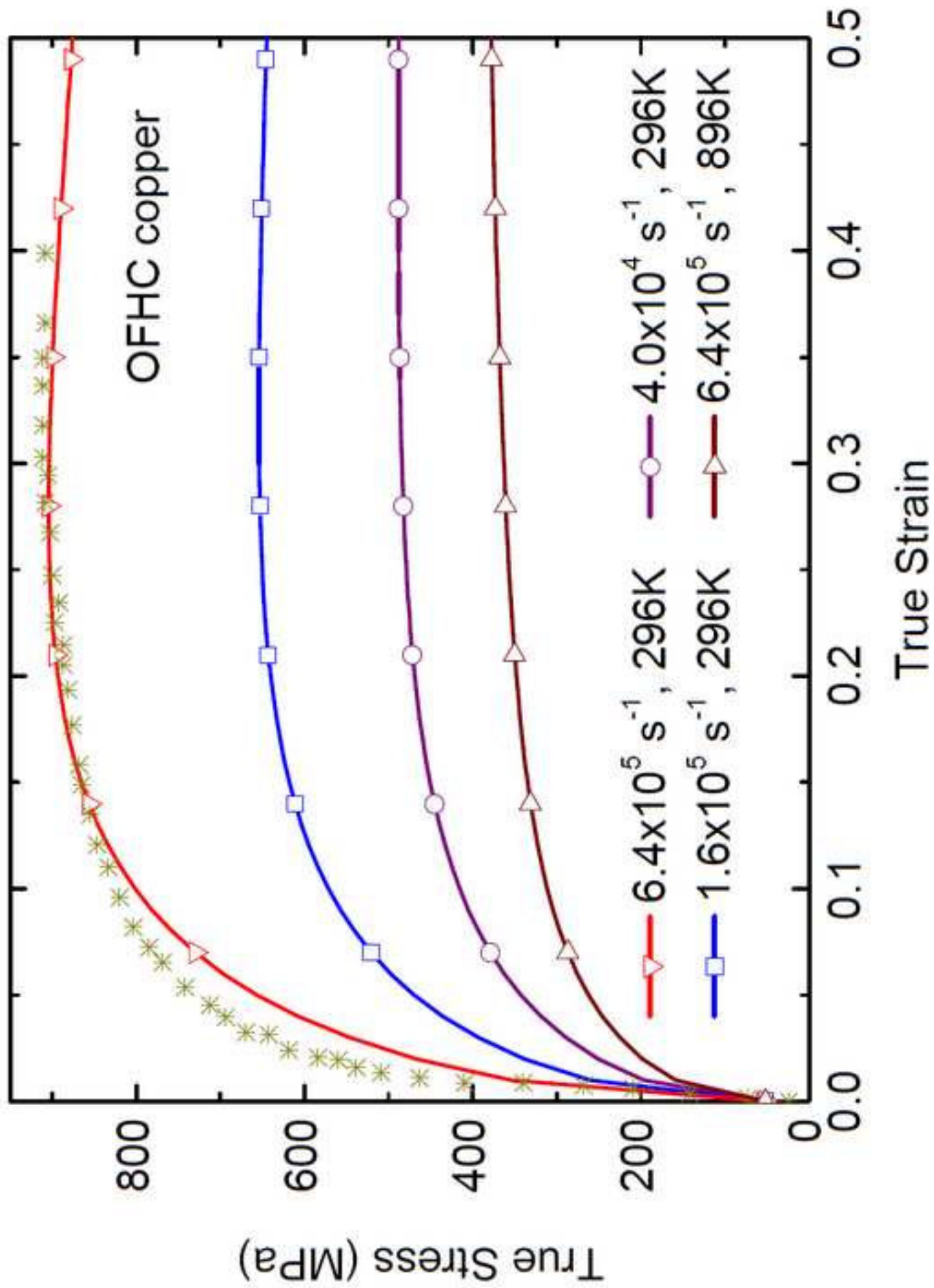


Figure 4

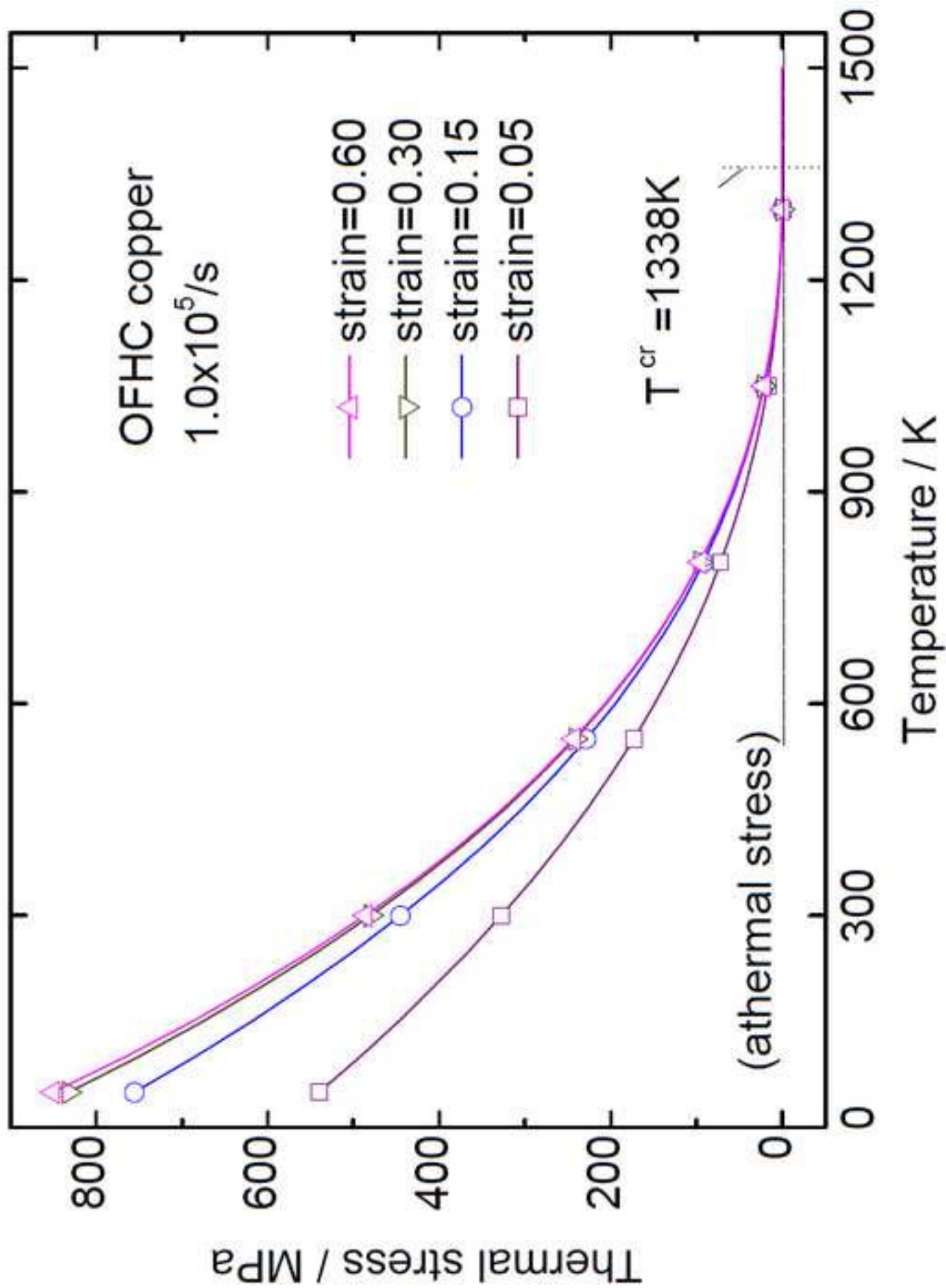


Figure 5

Table 1 Final optimized results of the constitutive parameters of OFHC copper

(a) For the new model of Eq. (21)

Constitutive parameters	Theoretically evaluated ranges	Optimized results	Unit
\hat{C}	$[1 \times 10^3, 1 \times 10^4]$	9850	<i>MPa</i>
k_0	[1, 10]	10	/
c_0	[0.1, 1]	0.483	/
c_1	$[1.8 \times 10^{-5}, 1.8 \times 10^{-4}]$	4.93×10^{-5}	1/ <i>K</i>
c_2	$[1.8 \times 10^{-5}, 1.8 \times 10^{-4}]$	1.0×10^{-4}	1/ <i>K</i>
p	(0, 1]	0.45	/
q	[1, 2]	1.0	/

(b) For the reduced model of Eq. (24)

Constitutive parameters	Theoretically evaluated ranges	Optimized results	Unit
\hat{C}	[100, 1000]	959	<i>MPa</i>
k_0	[0.1, 1]	0.82	/
c_2	$[1.8 \times 10^{-5}, 1.8 \times 10^{-4}]$	5.75×10^{-5}	1/ <i>K</i>
p	(0, 1]	0.91	/
q	[1, 2]	1.47	/

- Established a new constitutive model to describe the fcc polycrystalline plasticity at extremely high strain rates.
- Proposed a unified constitutive model which can predict precise flow stresses across a wide range of strain rates from $1 \times 10^{-4} s^{-1}$ to $6.4 \times 10^5 s^{-1}$.
- Explained the flow stress upturn phenomenon observed in experiments.

ACCEPTED MANUSCRIPT